HUNGARIAN UNIVERSITY OF
AGRICULTURE AND LIFE SCIENCES

The Effect of Integrating an Earth-Air Heat Exchanger on Photovoltaic Module Efficiency in Combination with a Solar Chimney

PhD Thesis

by
Mohammed Hussein Ali

Gödöllő
2024

Doctoral school

Denomination: Doctoral School of Mechanical Engineering

Science: Mechanical Engineering

Leader: Prof. Dr. Gábor Kalácska, DSc
Institute of Technology
Hungarian University of Agriculture and Life Sciences,
Gödöllő, Hungary

Supervisor: Prof. Dr. János Beke, DSc
Institute of Technology
Hungarian University of Agriculture and Life Sciences,
Gödöllő, Hungary

Co-Supervisor: Associate Prof. Dr. Zoltán Kurják, PhD
Institute of Technology
Hungarian University of Agriculture and Life Sciences,
Gödöllő, Hungary

…… ……

Affirmation of supervisor Affirmation of head of school

CONTENTS

1. INTRODUCTION, OBJECTIVES

Solar energy is fundamentally an inexhaustible source and potentially capable of meeting a significant portion of the world's future energy desires. It is the most promising unconventional energy source, particularly for contributing to low-temperature applications like Photovoltaic (PV) modules, solar thermal, and solar chimneys. The cost of solar energy has decreased fast in recent years. Solar energy can be generated in solar thermal power plants and PV modules. Moreover, there is another method, namely, the solar chimney (SC). This research investigates the integration of Earth-Air Heat Exchanger (EAHE) systems with SC to further enhance PV performance. EAHE provide cool air, mitigating the negative impact of high ambient temperatures on PV modules. The combined system aims to leverage the SC's ability to increase air velocity without external energy input, while the EAHE cools the modules, leading to an overall gain in energy output. While both PV modules and SC have their limitations, combining them with EAHE offers a promising hybrid approach. This concept, similar to hybrid solar-geothermal systems, seeks to exploit the complementary strengths of each technology to overcome individual drawbacks. Previous research exploring similar hybrid systems focused on utilizing geothermal energy to enhance SC efficiency. This study delves deeper, specifically investigating the impact of integrating EAHE within a PV-SC system. This novel approach has yet to be extensively explored, presenting exciting possibilities for boosting solar energy capture and utilization. The main objectives of the present work are to investigate the following:

- To examine the effect of thermo-physical properties of the multilayer soil on the earth-air heat exchanger efficiency.
- To develop a novel MATLAB simulation model to examine and construct the hybrid system using EAHE, SC, and PV modules. The model estimates global temperature gradients and thermo-physical features to aid future studies and save time, money, and effort.
- To study the effect of the geometric configuration on natural airflow generation in the integrated system consisting of PV module, SC, and EAHE. This airflow is used for cooling the PV modules.
- To determine how the forced airflow and earth-air heat exchanger affect the efficiency of the PV modules.
- To explore the effect of the solar air collector integrated with the hybrid system (PV, SC, EAHE) on the efficiency of the PV modules.
- To investigate how the efficiency of an earth-air heat exchanger system is affected by the geometric configuration of the system.

2. MATERIALS AND METHODS

Al-Najaf, renowned for its hot summers and mild winters, is chosen for its extreme climate, offering insights into the hybrid system's (PV modules, SC, and EAHE) performance under intense heat. Conversely, Gödöllő in Hungary has colder winters and milder summers, adding climatic diversity for a comprehensive system evaluation.

2.1. Experimentation

2.1.1. Soil Temperature Gradient Measurement

Soil temperature gradients were crucial for understanding heat transfer within the Earth. Sensors were placed at depths ranging from 1-5 m in Al-Najaf and 1-2 m in Gödöllő. Data collection occurred year-round, recording soil temperatures and ambient temperatures. In Al-Najaf, six thermocouples measured soil temperatures every ten minutes in 2019, while in Gödöllő, three thermocouples did the same every ten minutes from 2022-2023. A PVC pipe was used to prevent debris from entering the test pits. The schematic diagram illustrates the experimental setup at both sites.

2.1.2. Soil Thermo-physical Properties Measurement

The study aimed to develop an experimental method for measuring soil thermo-physical properties and their impact on EAHE performance. Properties like moisture content, thermal conductivity, specific heat capacity, and thermal diffusivity were measured. In Gödöllő, the area was excavated to 2 m, revealing five soil layers in terms of type and thickness. Soil samples from each layer were collected and preserved for analysis. Laboratory analysis using the Mettler-Toledo HE53 dryer determined the thermo-physical properties of the soil.

2.1.2.1. Single-layer Soil Thermo-physical Properties Measurement

Samples were prepared as appeared in Fig. 1, with initial volume and mass recorded before property measurement. Using a Moisture Analyzer, each sample was treated per instructions, and the final mass and volume were measured. This process provided data on moisture content, and wet and dry density, essential for calculating thermal conductivity, specific capacity, and thermal diffusivity.

Fig. 1. The five soil samples.

2.1.2.2. Multi-layered Soil Thermo-Physical Properties Measurement

This study proposes two new approaches to calculate and estimate thermo-thermal properties for multi-layer soil.

1- The new laboratory approaches

For measuring the equivalent thermo-physical properties of multilayer soil, all samples were combined based on the thickness ratio of each sample to the total trench depth as illustrated in Fig. 2. After careful laboratory analysis, the samples' thermal and physical properties were determined using the Moisture Analyzer device. Before measuring properties, the initial volume and mass of the sample were recorded. The sample was then processed individually inside the experimental device, and its final mass and volume were measured afterward. This process provided data on moisture content, wet density, and dry density, which were used to calculate sample density, thermal conductivity, specific heat capacity, and thermal diffusivity.

Fig. 2. The types of mixed soil layers according to the indicated percentages.

2- The new estimation approaches

the practical laboratory approach calls for all types of soil to be mixed, the amount of each type being proportional to its presence on the work site, and then subjected to standard procedures to examine their properties and use the following equations:

$$w_{eq} = \left(\frac{(M_T)_{be} - (M_T)_{af}}{(M_T)_{be}} \times 100 \right) \quad (1)$$

$$\rho_{eq,wet} = \left(\frac{(M_T)_{be}}{(V_T)_{be}} \right) \quad (2)$$

$$\rho_{eq,dry} = \left(\frac{(M_T)_{af}}{(V_T)_{af}} \right) \quad (3)$$

The theoretical simulation methodology can also be used by using the following equations to determine the equivalent moisture content if the sample size and mass for each type of soil removed and its moisture content are known:

$$w_{eq} = \left(w_1 \times \frac{t_1}{t_T} + w_2 \times \frac{t_2}{t_T} + w_3 \times \frac{t_3}{t_T} + w_4 \times \frac{t_4}{t_T} + w_5 \times \frac{t_5}{t_T} \right) \quad (4)$$

$$\rho_{eq,wet} = \left(\frac{(M_1 + M_2 + M_3 + M_4 + M_5)_{be}}{(V_1 + V_2 + V_3 + V_4 + V_5)_{be}} \right) \quad (5)$$

$$\rho_{eq,dry} = \left(\frac{(M_1 + M_2 + M_3 + M_4 + M_5)_{af}}{(V_1 + V_2 + V_3 + V_4 + V_5)_{af}} \right) \quad (6)$$

2.1.3. Earth-Air Heat Exchanger Performance Evaluation

EAHE was installed at a depth of 2 m in Gödöllő, Hungary, within a trench measuring 1 m wide, 2 m deep, and 14 m long. Two systems, EAHE-a and EAHE-b, were installed, each consisting of PVC pipes with a diameter of 0.1 m and a horizontal length of 10 m. These systems were connected to inclined pipes at an angle of 45° and a length of 3 m, with part of it inside the soil and part outside. Each system was divided into halves, with a vertical branch inside the soil, providing flexibility for comparison and study purposes. Seven temperature sensors were deployed, with one measuring ambient temperature and six placed at the inlet and outlet of each EAHE to monitor air temperature, enabling assessment of EAHE performance. Two anemometers were used to measure airflow velocity at both EAHE systems.

The data logger continuously recorded temperature and airflow velocity data. SmartDEN Logger and anemometer software were employed for temperature and airflow velocity recordings, respectively. The installation process involved digging and completing system installation. Fig. 3 illustrates a three-dimensional schematic of the proposed hybrid system, providing comprehensive details of the system layout.

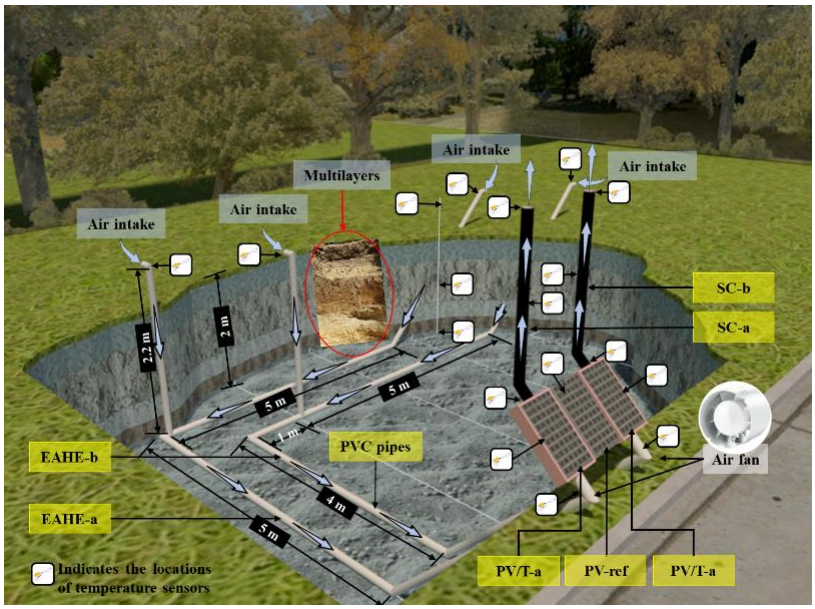

Fig. 3. The three-dimensional schematic of the proposed new hybrid system.

2.1.4. Integrated PV Module Performance Evaluation

Three monocrystalline PV modules (87TH424) were used for comparison, with a nominal power of 50 W and an area of 0.268 m². Two modules were used to construct PV/T models, incorporating a polystyrene sheet as thermal insulation to form ducts for air cooling. These were labeled PV/T-a and PV/T-b, connected to EAHE-a/SC-a and EAHE-b/SC-b, respectively. The third module, PV-ref, served as a reference and was not integrated with PV/T or connected to EAHE or SC. All three modules were installed with a tilt angle of 45° and an azimuth angle of -20°. Eight temperature sensors were deployed, including ambient temperature sensors and sensors at the inlet and outlet of PV/T-a and PV/T-b to monitor air temperature. Additional sensors were placed at the back of PV-a, PV-ref, and PV-b to monitor module temperatures. Photoelectric solar radiation sensors and electric wires connected to smart Arduino Denkovi-smart-32 were used to measure solar radiation, current, voltage, and temperatures. Data acquisition was conducted using smart Arduino Denkovi-smart-32, recording parameters at one-minute intervals. Desktop computers were utilized for real-time monitoring. SC, available in various sizes and configurations, was integrated into the system. It featured circular and rectangular tubes with hydraulic diameters of 0.1 m and lengths of 1.5 m. SC came in white and black colors. Figs. 4 and 5 provide visual representations of the fabrication process of PV/T models, and their installation on supporting structures.

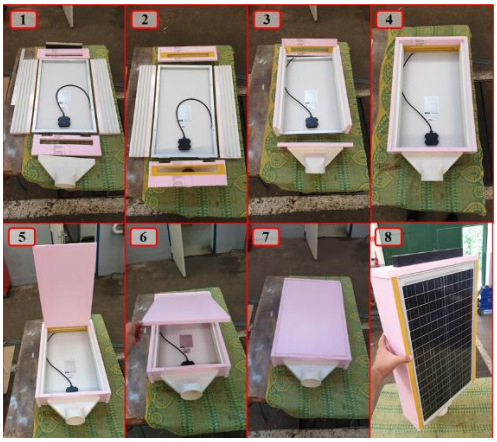

Fig. 4. The practical installation and manufacturing steps of the PV/T duct and PV modules.

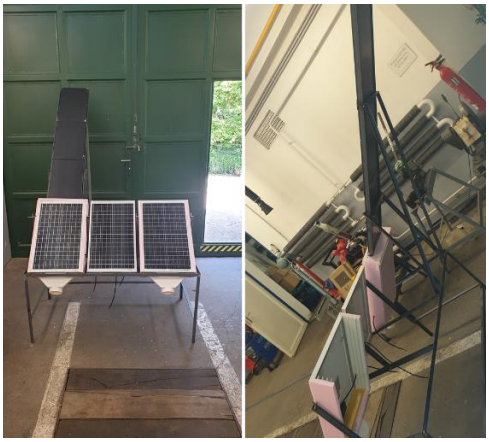

Fig. 5. The PV/T duct and PV modules are installed on the supporting iron structure.

2.1.5. Integrated Solar Chimney Performance Evaluation

Different types of SC were installed, including cylindrical and rectangular ones, with variations in color and shape. SCs were connected to PV/T-a and PV/T-b, labeled SC-a and SC-b respectively. SCs were vertically installed on supporting

structures. Five temperature sensors were used to monitor air temperature at SC-a and SC-b inlets and outlets. Data was recorded using a smart Arduino Denkovi-smart-32 every minute for real-time monitoring. Fig. 6 illustrates the installation of SC-a and SC-b on supporting structures.

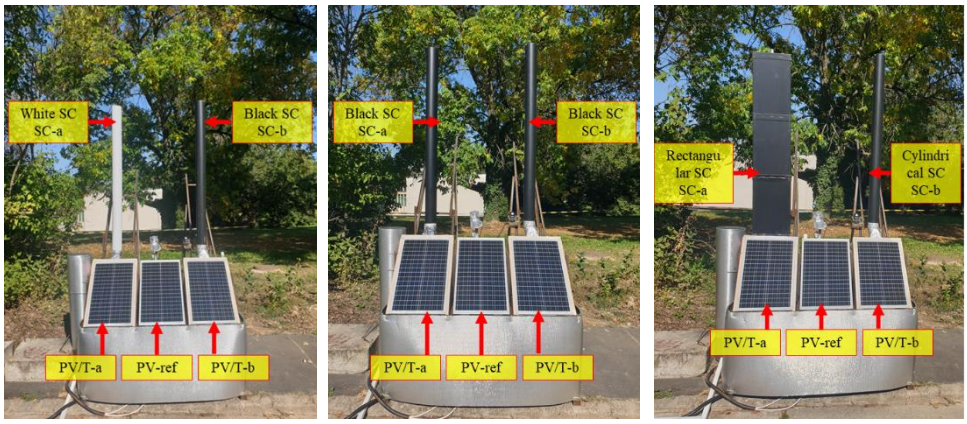

Fig. 6. The types of the examined solar chimneys.

2.2. Simulation Model Development

The study focuses on mathematical modeling for soil gradient and the EAHE. The EAHE utilizes buried pipes to cool incoming air through heat transfer with the ground. This cooled air is then circulated into a building or space, possibly via a PV module system. The study details the physical and thermal properties of air and PVC, essential for thermal analysis. Furthermore, it presents equations for soil temperature modeling, considering parameters like thermal conductivity and water content. The text also delves into the modeling of a SC system, emphasizing airflow behavior's significance for overall efficiency. Additionally, it outlines mathematical modeling for a PV module and a PV/T hybrid system, incorporating energy balance equations and factors influencing efficiency. The hybrid system integrates EAHE, SC, and PV technologies, with a Simulink model demonstrating its design and performance estimation capabilities. Overall, the study provides a comprehensive understanding of these renewable energy systems and their interactions, facilitating their effective utilization and optimization.

Soil properties that determine its response to temperature changes at the surface are volumetric heat capacity, C_v, soil thermal conductivity, k_{soil}, and water content (moisture), w. The method for sizing the EAHE requires knowledge of the minimum and maximum ground temperature at the EAHE depth. The undisturbed ground temperature, T_{soil}, expressed in °C, can be calculated using:

$$T_{soil}(z,t) = T_{mean} + A_o \exp(-z/d) \left[\sin\left((2\pi (t - t_o) / 365) - (z / d) - (\pi / 2)\right)\right] \quad (7)$$

In which T_{soil} (z,t) denotes the temperature of the soil at time t (day) and depth z (m), T_{mean} defines the average ambient temperature (^oC), A_o connotes the annual amplitude of the ambient temperature (^oC), d is the damping depth (m) of annual fluctuation and t_o is the time lag (days) between an arbitrary starting date (considered as Jan. 1).

Because heat conducts more quickly as compared to thermal mass, a high thermal diffusivity value is desired. To determine these thermal characteristics, Eqs. ((8)-(11)) have been utilized to develop analytical equations:

$$k_{soil}= 0.14423\ (0.9 \log (w) - 0.2)\ 10^{\ 0.000642\ \rho_d} \quad \text{(For silt and clay soils)} \qquad (8)$$

$$k_{soil}= 0.14423\ (0.7 \log (w) + 0.4)\ 10^{\ 0.000642\ \rho_d} \quad \text{(For sand soil)} \qquad (9)$$

In this equation, ρ_d is the dry soil density. The adjusted specific heat capacity of soil may be calculated as follows:

$$C_{p,soil} = \frac{[w\ C_{pw} + (100 - w)\ C_{pd}]}{100} \qquad (10)$$

C_{pw} is water's specific heat capacity (4180 J/kg.K). C_{pd} is the soil's dry specific heat capacity (840 J/kg.K). The corrected density of soil may be given by:

$$\rho_{soil} = \frac{[w\ \rho_w + (100 - w)\ \rho_d]}{100} \qquad (11)$$

ρ_w is the density of water. The final form of the MATLAB Simulation model is illustrated in Fig. 7.

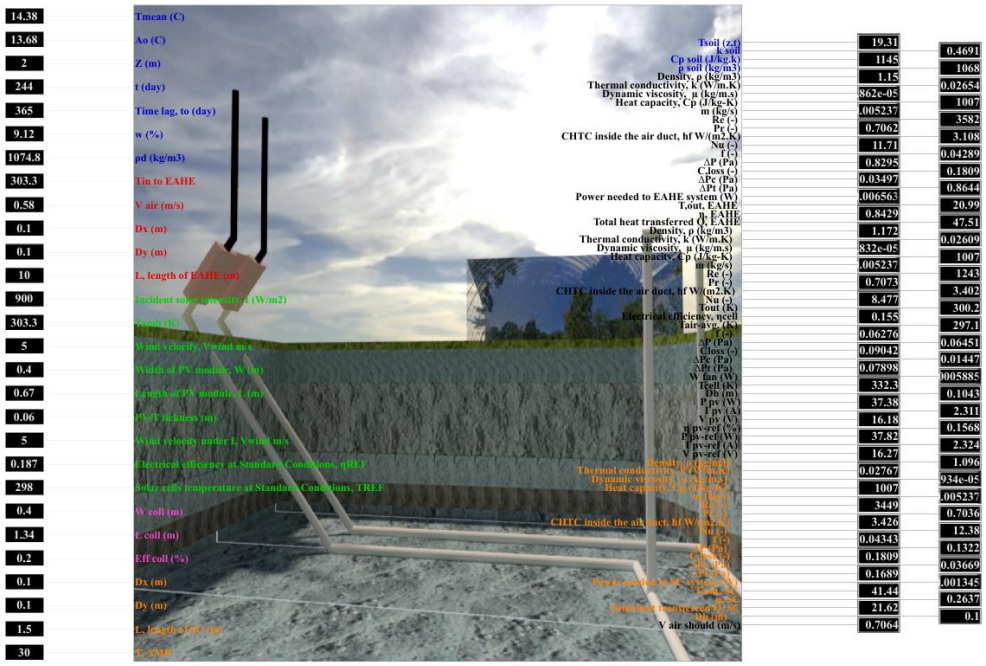

Fig. 7. Simulink model of the hybrid system.

3. RESULTS

3.1. Model Validation and Analysis

The figures display measured and simulated data for various parameters, including soil temperature, outlet air temperature of EAHE, PV module temperatures, SC temperatures, and power produced by PV modules. Discrepancies between measured and simulated data are observed, ranging from (5.0-6.9)% on average, with some variations in specific cases. Despite these differences, the percentage of difference remains generally acceptable, not exceeding 6.4%. These variations may stem from factors such as measurement accuracy, simulation model precision, and environmental conditions. However, the reliability of the simulation model, built using MATLAB, is affirmed, as it offers valuable insights for future system implementations with the potential for further refinement.

3.2. Soil Temperature and Thermo-Physical Properties

In Al-Najaf, soil temperatures at a depth of 1 meter range from 14.9 °C in January to 36.3°C in July. In Gödöllő, soil temperatures at the same depth range from 6 °C in January to 21.2 °C in July. In Al-Najaf, soil temperatures at a depth of 2 meters range from 18.2 °C in January to 32.9 °C in June. In Gödöllő, soil temperatures at the same depth range from 10.3°C in January to 17.8°C in August.

The amount of the relative difference between the outlet temperature of the EAHE system is 3.8% for a system of length 12 m and the thermal diffusivity range between 3.0258E-07 m^2/s and 4.3171E-07 m^2/s. It is subject to the following equation: $RD_{T,out}$ represents the relative difference of the outlet temperature, while L_{pipe} represents the length of the EAHE pipe. The effect of the relative difference in the type of layers was directly proportional to the length of the EAHE. As the length of the EAHE increases, the relative difference increases. Fig. 8. displays air temperatures along the EAHE pipe in six different cases.

$$RD_{T,out}=0.0002389\times L_{pipe}^{\ 3}-0.01877\times L_{pipe}^{\ 2}+0.5089\times L_{pipe}-0.09124,\ R^2=0.99 \quad (12)$$

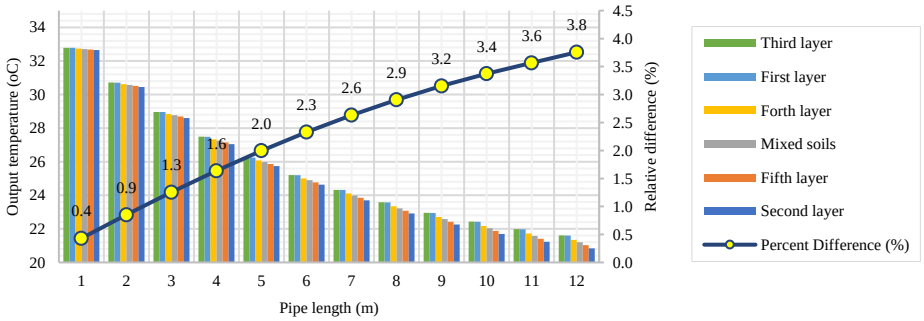

Fig. 8. The air temperature along the pipe of the six cases.

3.3. Earth-Air Heat Exchanger Performance

The cooling mode experiment demonstrated consistent performance, with the system maintaining an efficiency around 71% throughout the day. In the heating mode, the EAHE effectively raised air temperature, maintaining efficiency at approximately 70% throughout the day. The MS-EAHE has the lowest pressure loss among other EAHE system types, resulting in the least additional air fan power required to operate the fan needed to circulate the air inside it. M-EAHE had more significant pressure losses compared to MS-EAHE by approximately 1.6 times. The S-EAHE and TS-EAHE types had the highest pressure losses. They required the most significant amount of additional air fan power for operation, as their pressure losses were 13.8 and 14.7 times, respectively, and their additional air fan power was 71.1 and 75.5 times higher than MS-EAHE. Furthermore, the S-EAHE and TS-EAHE have the highest cooling potential compared to other EAHE system types, at 278.3 W on average. The MS-EAHE and the M-EAHE have less cooling potential of 19.1% and 22.3%, respectively, compared to the S-EAHE and the TS-EAHE types. The four types are subject to the following equations. CP represents the cooling potential and T_{in} represents the inlet temperature of the EAHE. As illustrated in Figs. 9 and 10.

$$CP = 1.853\times10^{4}\ sin(0.002276\ T_{in} + 6.218), \quad R^2=1 \quad \text{(For S-EAHE and TS-EAHE)} \quad (13)$$

$$CP = 1.295\times10^{4}\ sin(0.002528\ T_{in} + 6.211), \quad R^2=1 \quad \text{(For M-EAHE)} \quad (14)$$

$$CP = 1.383\times10^{4}\ sin(0.002467\ T_{in} + 6.213), \quad R^2=1 \quad \text{(For MS-EAHE)} \quad (15)$$

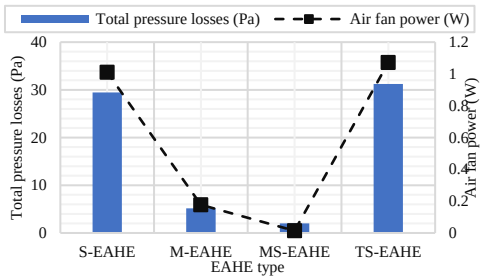

Fig. 9. The pressure losses and air fan power as a function of EAHE types.

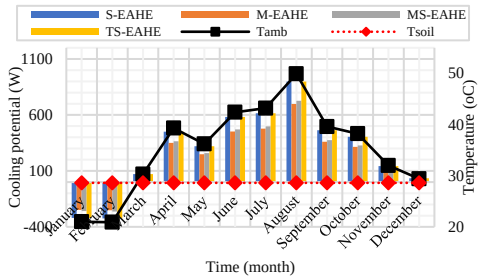

Fig. 10. The cooling potential and T_{in} of EAHE types as a function of time.

3.4. The performance of the PV module depends on the natural ventilation

3.4.1. Investigation of the effect of the solar chimney on the PV module efficiency

Combining SC with the PV module and EAHE increases the airflow velocity inside the EAHE tube up to 5.3 times compared to not combining them. The average $P_{PV\text{-}a}$ and $P_{PV\text{-}b}$ achieved were 35.1 W and 34.5 W, respectively. The

power increase produced by PV-ref was higher by 1.7 % and 3.5 % than by the PV-a and PV-b modules, respectively. The PV-ref was the most efficient compared to PV-a and PV-b. The average efficiency achieved by PV-ref, PV-a, and PV-b was 15.9%, 15.6%, and 15.4%, respectively. As illustrated in Figs. 11 and 12. The airflow velocity is subjected to the following equation because of this integration:

$$v_{air} = 2.807 - 0.003708\, I - 0.06196\, T_{amb} + 1.005\times10^{-6}\, I^2 + 7.783\times10^{-5}\, I\, T_{amb} - 0.0002501\, T_{amb}{}^2, \quad R^2 = 0.9623 \tag{16}$$

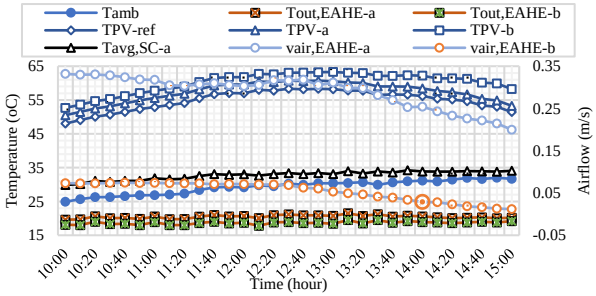

Fig. 11. The variation of T_{amb} vs. $T_{out,\ EAHE\text{-}a}$, $T_{out,\ EAHE\text{-}b}$, $T_{PV\text{-}ref}$, $T_{PV\text{-}a}$, $T_{PV\text{-}b}$, and $T_{avg,\ SC\text{-}a}$ and air velocity of the PV/T-a and PV/T- during the test time (Natural airflow - Case 1).

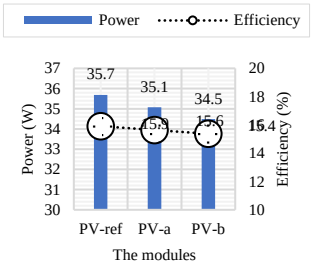

Fig. 12. The efficiency and power produced by the PV modules (Natural airflow - Case 1).

3.4.2. Investigation of the effect of solar chimney color on the PV module efficiency

The dark-colored SC (black) absorbs an amount of radiation, which increases the amount of heat generated inside it, and thus the velocity of airflow inside the EAHE tube increases, but the amount of this increase does not exceed 1% compared to using a white-colored SC. The average $P_{PV\text{-}b}$ and $P_{PV\text{-}a}$ achieved were 34.2 W and 34.1 W, respectively. The power increase produced by $P_{V\text{-}ref}$ was higher by 1.6 % and 1.7 % than by the PV-b and PV-a modules, respectively. The PV-ref was the most efficient compared to PV-a and PV-b. The average efficiency of PV-ref, PV-b, and TPV-a achieved were 16%, 15.74%, and 15.73% respectively, as illustrated in Figs. 13 and 14.

3.4.3. Investigation of the effect of solar chimney shape on the PV module efficiency

Using a rectangular SC increases the area facing sunlight, which leads to it absorbing a greater amount of radiation, which increases the amount of heat generated inside it. Therefore, the airflow velocity inside the EAHE tube rises to 5% compared to using a circular SC, which increases the possibility of improving the efficiency of the PV module during natural airflow using a rectangular SC. The average $P_{PV\text{-}a}$ and $P_{PV\text{-}b}$ were 34.2 W and 34.2 W, respectively. The increase in energy produced by PV modules was 1.64% and 1.6% higher compared to PV-

b and PV-a modules, respectively. The PV-ref was the most efficient compared to PV-a and PV-b. The average efficiency of PV-ref, PV-a, and PV-b achieved were 15.9%, 15.8%, and 15.7% respectively, as illustrated in Figs. 15 and 16. To estimate the velocity of the airflow, the following equation is applied:

$$v_{air} = -0.746 + 0.001783\, I + 0.02385\, T_{amb} + 8.364\times10^{-8}\, I^2 - 4.812\times10^{-5}\, I\, T_{amb}, \quad R^2 = 0.9789 \qquad (17)$$

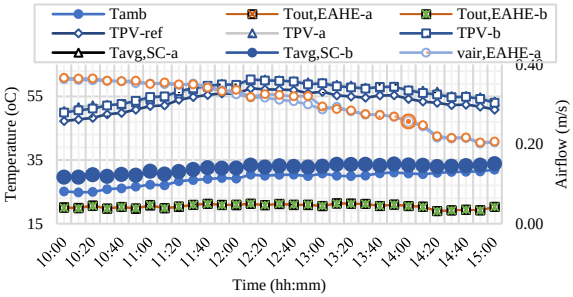

Fig. 13. The variation of T_{amb} vs. $T_{out,\ EAHE\text{-}a}$, $T_{out,\ EAHE\text{-}b}$, $T_{PV\text{-}ref}$, $T_{PV\text{-}a}$, $T_{PV\text{-}b}$, $T_{avg,\ SC\text{-}a}$ and $T_{avg,\ SC\text{-}b}$ and air velocity of the PV/T-a and PV/T- during the test time (Natural airflow - Case 2).

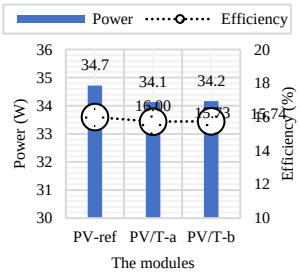

Fig. 14. The efficiency and power produced by the PV modules (Natural airflow - Case 2).

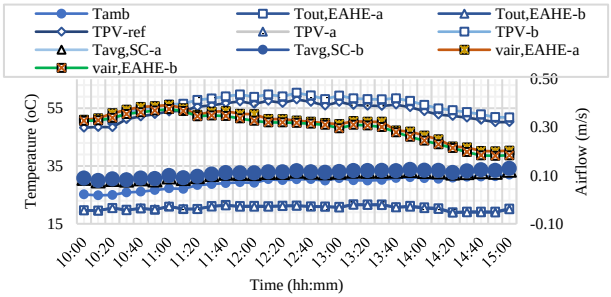

Fig. 15. The variation of T_{amb} vs. $T_{out,\ EAHE\text{-}a}$, $T_{out,\ EAHE\text{-}b}$, $T_{PV\text{-}ref}$, $T_{PV\text{-}a}$, $T_{PV\text{-}b}$, $T_{avg,\ SC\text{-}a}$ and $T_{avg,\ SC\text{-}b}$ and air velocity of the PV/T-a and PV/T- during the test time (Natural airflow - Case 3).

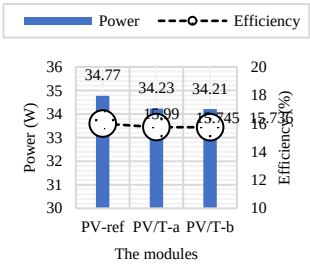

Fig. 16. The efficiency and power produced by the PV modules (Natural airflow - Case 3).

3.4.4. *Investigation of the effect of EAHE system length on the PV module efficiency*

The natural airflow (caused by the SC) that occurs inside the EAHE is affected by its length. The airflow velocity generated in shorter EAHEs (EAHE= 5 m) is 14.7% faster than in longer EAHE (EAHE= 10 m). The average $P_{PV\text{-}b}$ and $P_{PV\text{-}a}$ were 35.31 W and 35.29 W, respectively. The increase in energy produced by PV modules was 1.7% and 1.6% higher than PV-b and PV-a modules, respectively. The PV-ref was the most efficient compared to PV-a and PV-b. The average efficiency of PV-ref, PV-a, and PV-b achieved were 16%, 15.73%, and 15.74%

respectively, as illustrated in Figs. 17 and 18. The following equation establishes the airflow velocity:

$$v_{air} = -2.173 + 0.001843\, I + 0.1288\, T_{amb} - 4.726\times10^{-5}\, I\, T_{amb} - 0.001891\, T_{amb}^{\,2}, \quad R^2 = 0.9731 \qquad (18)$$

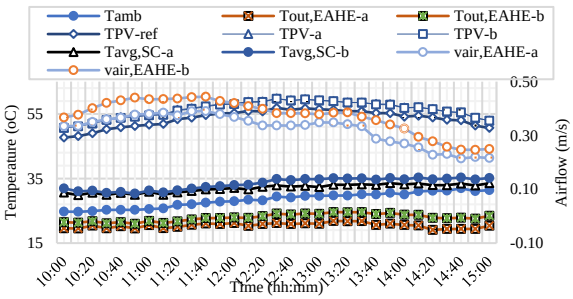

Fig. 17. The variation of T_{amb} vs. $T_{out,\ EAHE\text{-}a}$, $T_{out,\ EAHE\text{-}b}$, $T_{PV\text{-}ref}$, $T_{PV\text{-}a}$, $T_{PV\text{-}b}$, $T_{avg,\ SC\text{-}a}$ and $T_{avg,\ SC\text{-}b}$ and air velocity of the PV/T-a and PV/T- during the test time (Natural airflow - Case 4).

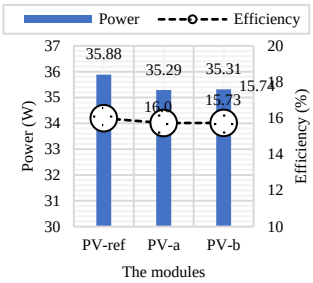

Fig. 18. The efficiency and power produced by the PV modules (Natural airflow - Case 4).

3.4.5. Investigation of the effect of the depth of PV/T ducts on the efficiency of the PV module

The airflow velocity that passes through a narrower PV/T collector is 1.2 times higher than the airflow that passes through a wider PV/T collector. It is necessary to make use of the following equation to determine the velocity of the airflow:

$$v_{air} = 1.696 + 0.003903\, I - 0.2162\, T_{amb} - 7.523\times10^{-7}\, I^2 - 6.719\times10^{-5}\, I\, T_{amb} + 0.004525\, T_{amb}^{\,2}, R^2 = 0.9617 \qquad (19)$$

The average $P_{PV\text{-}a}$ and $P_{PV\text{-}b}$ were 36.4 W and 36.6 W, respectively. The increase in energy produced by the PV-ref module was 1.2% and 1.7% higher than the PV-b and the PV-a modules, respectively. The PV-ref was the most efficient compared to PV-a and PV-b. The average efficiency achieved by PV-ref, PV-a, and PV-b was 15.9%, 15.6%, and 15.7%, respectively, as illustrated in Figs. 19 and 20.

3.4.6. Investigation of the effect of the Earth-Air Heat Exchanger on the PV module efficiency

The airflow velocity generated by the SC combined with the PV module is 252.3% faster than the airflow velocity generated by the SC combined with the PV module and EAHE. Although the efficiency of the EAHE was 90.8%, this did not improve the efficiency of the PV module integrated with it. The efficiency of the PV module integrated with it was 15.4%. In comparison, the efficiency of the PV module integrated with the SC was somewhat better at 15.5% due to the low flow velocity resulting from the low pressure inside the EAHE tubes. The average $P_{PV\text{-}a}$ and $P_{PV\text{-}b}$ were 33.5 W and 33.7 W, respectively. The increase in energy

produced by PV-ref modules was 1.7% and 1% higher compared to PV-b and PV-a modules. As illustrated in Figs. 21 and 22. The airflow velocity is subjected to the following equation:

$$v_{air} = -228.3 + 0.9259\, I + 5.233\, T_{amb} - 0.001332\, I^2 - 0.01941\, I\, T_{amb} + 7.847\times10^{-7}\, I^3 + 2.384\times10^{-5}\, I^2\, T_{amb} - 1.481\times10^{-10}\, I^4 - 9.713\times10^{-9}\, I^3\, T_{amb},\ R^2 = 0.8699 \quad (20)$$

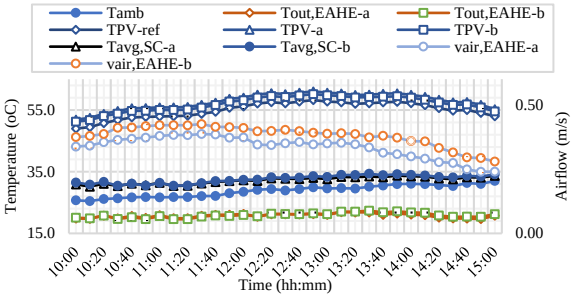

Fig. 19. The variation of T_{amb} vs. $T_{out,\ EAHE\text{-}a}$, $T_{out,\ EAHE\text{-}b}$, $T_{PV\text{-}ref}$, $T_{PV\text{-}a}$, $T_{PV\text{-}b}$, and $T_{avg,\ SC\text{-}a}$ and air velocity of the PV/T-a and PV/T- during the test time (Natural airflow - Case 5).

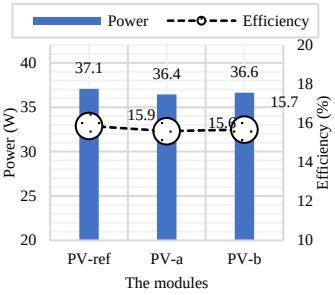

Fig. 20. The efficiency and power produced by the PV modules (Natural airflow - Case 5).

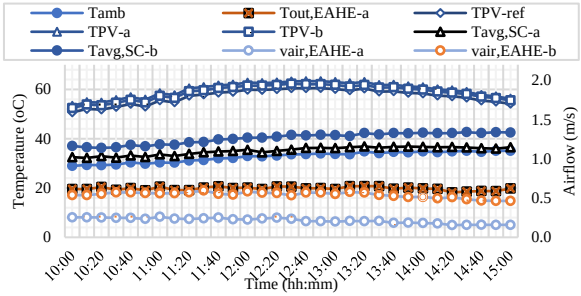

Fig. 21. The variation of T_{amb} vs. $T_{out,\ EAHE\text{-}a}$, $T_{PV\text{-}ref}$, $T_{PV\text{-}a}$, $T_{PV\text{-}b}$, and $T_{avg,\ SC\text{-}a}$ and air velocity of the PV/T-a and PV/T- during the test time (Natural airflow - Case 6).

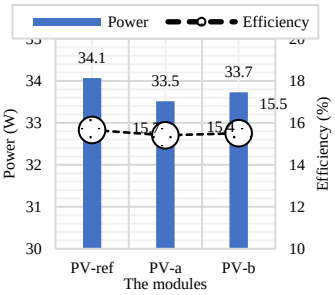

Fig. 22. The efficiency and power produced by the PV modules (Natural airflow - Case 6).

3.5. The performance of the PV module depends on the forced ventilation

The velocity generated naturally by the SC alone (without additional SAC) is insufficient to generate sufficient airflow to cool the integrated PV module. It is necessary to integrate the hybrid system (PV-SC-EAHE) with forced air flow using fans, and this would cause an increase in the electrical power generated by the integrated PV modules. However, the forced speed must not be less than 1 m/s or 1.5 m/s, as the increase in generated power is not less than 37.12 W and 35.39 W (achieving an increased power of no less than 0.37 W and 0.84 W) respectively. In this case, the power was generated from the PV modules, but at the same time, power was consumed from another source to operate the fans,

which is not less than 3 W at a fan speed of 1 m/s and 4.6 W at a fan speed of 1.5 m/s. Figs. 23, 24, and 25 illustrated the efficiency and power produced by the PV modules at forced airflow were 0.5, 1, and 1.5 m/s) The additional power generated by the integrated PV module was subject to the following equation:

$$P_{pv\text{-}add} = P_{pv} - P_{pv\text{-}ref} = -0.7054 + 1.087 \times v_{fan} - 0.02717\, P_{fan}\ ,\ R^2 = 0.9999 \quad (21)$$

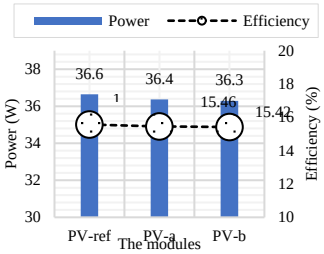

Fig. 23. The PV efficiency and power (Forced airflow - Case 1).

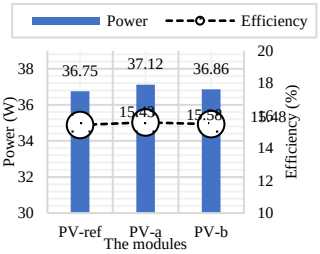

Fig. 24. The PV efficiency and power (Forced airflow - Case 2).

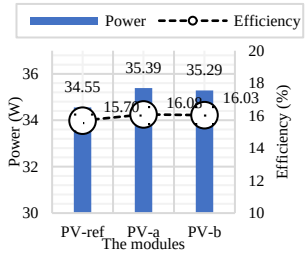

Fig. 25. The PV efficiency and power (Forced airflow - Case 3).

3.6. The performance of the PV module depends on the solar air collector

3.6.1. Investigation of the effect of solar collectors on the efficiency of PV module

The temperature of the air exiting the PV/T collector and entering the SC is not sufficient to create an adequate flow to draw air from the EAHE, passing through the PV/T, and reaching the SC. This requires raising the temperature of the air before it enters the SC by incorporating a SAC. Therefore, the airflow velocity is directly proportional to the length of the SAC, which means that as the length of the SAC increases, the airflow rate increases and is subject to the equation:

$$v_{air} = 0.0599\, L_{coll} + 0.4564\ ,\quad R^2 = 0.9819 \quad (22)$$

The airflow rate was 0.47 m/s when the length of the collector was equal to the length of the PV module. When the length of the solar collector became ten times the length of the PV module, the velocity became equal to 1.03 m/s, which is sufficient at this value to sufficiently cool the PV module and increase the amount of power output compared to the non-integrated PV module.

The amount of power output from the PV module increased with the increase in the length of the SAC, as its amount was 37.38 W when the length of the collector was equal to the length of the PV module. Still, when the length of the collector was ten times the length of the PV module, the power increased by 2.2%. The generated power and temperature of the PV module with the SAC and the hybrid system (PV-SC-EAHE) are governed by the following equations respectively.

$$P_{PV} = 37.335\, L_{coll}^{0.0077}\ ,\quad R^2 = 0.9822 \quad (23)$$

$$T_{PV} = 0.0226\, {L_{coll}}^2 - 0.5569\, L_{coll} + 59.326\ ,\quad R^2 = 0.9983 \quad (24)$$

Fig. 26 shows the relationship between the length of the SAC and the airflow rate through the SC as a result of using the SAC. Fig. 27 shows the relationship between the length of the SAC compared to the generated power and the temperature of the PV module.

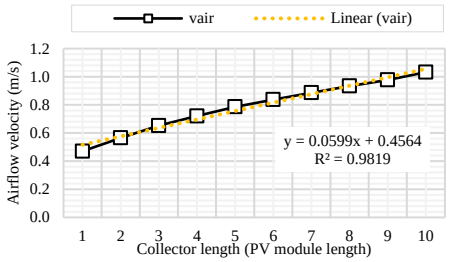

Fig. 26. The airflow velocity generated in the combined-assisted solar collector system is a function of the length of the PV module.

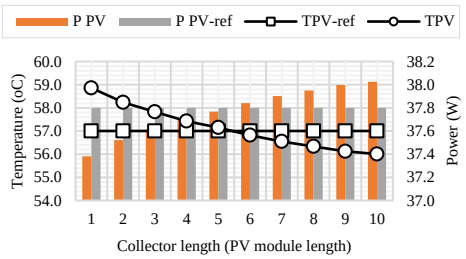

Fig. 27. The average PV power production by the PV modules and their temperatures.

3.6.2. *The effect of solar air collectors on the efficiency of the photovoltaic module in different climates*

The flow was 20% faster in the hot location (Al-Najaf) than in the cold location (Godollo). The generated velocity reached a maximum of 1.1 m/s in the hot location and 0.95 m/s in the cold location. Likewise, the flow increases more during the hot months of the year than in the cold months of the year in both climates (Fig. 28). The PV module temperatures in hot regions are generally higher compared to cold regions. The integrated PV module shows lower temperatures compared to the reference PV module in Al-Najaf and Godullo in all months. However, it is noted that the amount of cooling in hot areas was higher and better than in cold areas (2%) because the flow velocity was higher in the cold region (Fig. 29). The following equation is put into effect to the airflow velocities to perform the estimation:

$$v_{air} = 0.2762 + 0.005205\, I - 0.0423\, T_{amb} - 1.158\times10^{-5}\, I^2 + 0.0001367\, I\, V + 8.533\times10^{-9}\, I^3 - 1.166\times10^{-7}\, I^2\, T_{amb}, \quad R^2 = 0.9627 \tag{25}$$

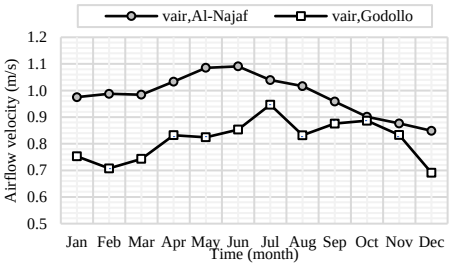

Fig. 28. The monthly naturally generated airflow velocity in Al-Najaf and Gödöllő.

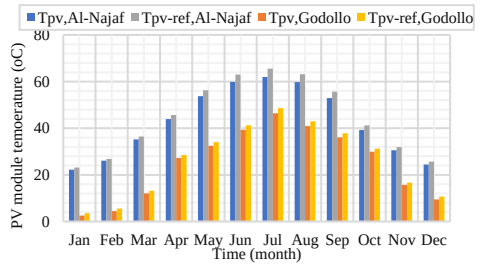

Fig. 29. The monthly PV temperatures of the integrated PV module compared to the PV_{-ref} for Al-Najaf and Gödöllő.

4. CONCLUSION AND SUGGESTIONS

The study investigated the integration of a photovoltaic (PV) module with a solar chimney (SC) and earth-air heat exchanger (EAHE) to enhance system efficiency. Conducted through experiments and simulations in Iraq (hot climate) and Hungary (cold climate), the research introduced a MATLAB/Simulink model for predicting soil temperature distribution and designing integrated or individual EAHE, SC, and PV systems.

Key findings include the introduction of innovative approaches assessing soil thermo-physical properties, demonstrating the model's reliability with a 93.6% match to measured data. Among four EAHE types, MS-pipe EAHE exhibited the lowest pressure losses and air fan power, while TS-pipe EAHE had the highest. S-pipe and TS-pipe EAHE showed the highest cooling potential, and multi-pipe EAHE had the lowest. SC integration increased airflow velocity by 5.2 times, with a rectangular SC enhancing velocity by 5% over a circular SC. The black SC exhibited a 1% higher airflow velocity than the white SC. EAHE length influenced natural airflow, with EAHE-5 m generating 14.7% faster velocity than EAHE-10 m.

In the case of narrower PV/T in EAHE, tube airflow velocity was 1.2 times that of wider PV/T. The SC with PV module achieved 252.3% faster airflow than the SC with PV module and EAHE. However, the PV module could not be cooled by SC's natural airflow alone, necessitating the integration of a solar air collector (SAC) before SC and after PV/T. Integrating a SAC 10 times the PV module's size increased PV module efficiency by 2.2%. Natural airflow in the hot location was 20% faster than in the cold location, reaching 1.1 m/s in the hot location and 0.95 m/s in the cold. Temperature differentials between ambient air and soil were observed, with stable soil temperatures at 5 m depth in Al-Najaf.

EAHE in Gödöllő demonstrated cooling and heating efficiency of 71% and 70.1%, respectively, lowering summer temperatures by 11°C and raising winter temperatures by 6.5°C. The study suggested further exploration of variables, such as integrating a solar dryer with the system, utilizing EAHE for night cooling and heating, and optimizing PV/T, SAC, SC, and EAHE structures. Opportunities for additional renewable energy sources, energy storage integration, and global impact assessment were proposed. Economic analysis of the long-term cost and benefits of the PV-SC-EAHE system was recommended for further research.

5. NEW SCIENTIFIC RESULTS

This section presents the new scientific findings from this research work as follows:

1. *The effect of thermo-physical properties of the multilayer soil on earth-air heat exchanger efficiency*

I discovered that the multi-layer soil affects the efficiency of the EAHE. Based on the experimental results, I found that the amount of the relative difference between the outlet temperature of the EAHE system is 3.8% for a system of length 12 m and the thermal diffusivity range between 3.0258E-07 m^2/s and 4.3171E-07 m^2/s. It is subject to the following equation: $RD_{T,out}$ represents the relative difference of the outlet temperature, while L_{pipe} represents the length of the EAHE pipe. The effect of the relative difference in the type of layers was directly proportional to the length of the EAHE. As the length of the EAHE increases, the relative difference increases.

$$RD_{T,out} = 0.0002389 \times L_{pipe}^{\,3} - 0.01877 \times L_{pipe}^{\,2} + 0.5089 \times L_{pipe} - 0.09124, \quad R^2 = 0.9999$$

For this reason, it was necessary to develop a new methodology to estimate the thermo-physical properties of the multi-layered soil, especially since the method adopted so far by researchers and engineers when estimating the temperature distribution of soil assumes that the soil is one layer, and this is not available in most locations around the world. Soil thermo-physical properties include specific heat capacity, thermal conductivity, density, which depends on moisture content and dry and wet density.

Accordingly, a practical laboratory method and a theoretical simulation method were developed as a general rule; the practical laboratory approach calls for all types of soil to be mixed, the amount of each type being proportional to its presence on the work site, and then subjected to standard procedures to examine their properties and use the following equations:

$$w_{eq} = \left(\frac{(M_T)_{be} - (M_T)_{af}}{(M_T)_{be}} \times 100 \right)$$

$$\rho_{eq,wet} = \left(\frac{(M_T)_{be}}{(V_T)_{be}} \right)$$

$$\rho_{eq,dry} = \left(\frac{(M_T)_{af}}{(V_T)_{af}} \right)$$

The theoretical simulation methodology can also be used by using the following equations to determine the equivalent moisture content if the sample size and mass for each type of soil removed and its moisture content are known:

$$w_{eq} = \left(w_1 \times \frac{t_1}{t_T} + w_2 \times \frac{t_2}{t_T} + w_3 \times \frac{t_3}{t_T} + w_4 \times \frac{t_4}{t_T} + w_5 \times \frac{t_5}{t_T} + \ldots\ldots + w_n \times \frac{t_n}{t_T}\right)$$

$$\rho_{eq,wet} = \left(\frac{(M_1 + M_2 + M_3 + M_4 + M_5 + \ldots\ldots + M_n)_{be}}{(V_1 + V_2 + V_3 + V_4 + V_5 + \ldots\ldots + V_n)_{be}}\right)$$

$$\rho_{eq,dry} = \left(\frac{(M_1 + M_2 + M_3 + M_4 + M_5 + \ldots\ldots + M_n)_{af}}{(V_1 + V_2 + V_3 + V_4 + V_5 + \ldots\ldots + V_n)_{af}}\right)$$

2. *Performance assessment of the integrated solar energy system with earth-air heat exchanger system.*

I have created the mathematical and programming linkage of equations and formulas critical for the design, evaluation, and analysis of an integrated solar energy system with EAHE (PV-SC-EAHE), with the aim of assisting designers and researchers in the task of visualizing and estimating the performance of a complex system across different global locations. This model is extremely important, as it not only facilitates the determination of the optimal length of the tube and ground area necessary to bury the tube to achieve the required air cooling of the integrated PV module and SC, but also provides valuable explanations about the basic mathematical relationships that manage the system.

The model is implemented using the MATLAB/Simulink environment, this model brings together a comprehensive set of crucial mathematical equations and formulas, which are complexly related both mathematically and programmatically. This allows designers across the world to evaluate soil temperature distribution at a variety of depths, estimate the thermo-physical properties of the soil at a specific location, as well as evaluate the temperature, efficiency, and power of the PV module. The model also provides assistance in determining the SC dimensions needed to ensure adequate airflow, drawing air from the surroundings through the integrated EAHE, PV and SAC system to enhance the use of solar energy. In addition, it provides a means of checking the temperature of the air entering the SC, forcing it out into the surrounding environment.

The provided and discussed measured and anticipated findings showed that the disparities between the two ranged from (6.0-6.9)%, with an average of 6.4%. These ratios are acceptable due to their capabilities, advantages, and cost savings in light of the measurement process, its challenges, and instantaneous and continuous weather fluctuations, as well as the conditions and assumptions that accompany the simulation model-building process using MATLAB. They are dependable vision and visualization tools. Since it was constructed using authorized scientific procedures and processes, the future system can alter and analyze its results before implementing it. Thus, this concept is promising and can be modified and developed in the future.

3. *Effect of geometric configuration on natural airflow generation in the integrated solar energy system with an earth-air heat exchanger system.*

I have explored the effect of the integration of SC and its shape, the integration of the EAHE and its length, PV/T depth, and the effect of climate on natural ventilation and air circulation during a hybrid system (PV-SC-EAHE). Based on the experimental results, the following are the outcomes that I have investigated:

- The SC, when integrated with PV modules and EAHE, leads to an increase of approximately 5.3 times in the airflow velocity. The airflow velocity is subjected to the following equation because of this integration:

$$v_{air} = 2.807 - 0.003708\, I - 0.06196\, T_{amb} + 1.005\times10^{-6}\, I^2 + 7.783\times10^{-5}\, I\, T_{amb} - 0.0002501\, T_{amb}^{\,2},\ R^2 = 0.9623$$

- The airflow velocity is increased by about 5% when the rectangular SC is utilized, as compared to the cylindrical SC. In order to estimate the velocity of the airflow, the following equation is applied:

$$v_{air} = -0.746 + 0.001783\, I + 0.02385\, T_{amb} + 8.364\times10^{-8}\, I^2 - 4.812\times10^{-5}\, I\, T_{amb},\quad R^2 = 0.9789$$

- The velocity of the airflow that passes through a narrower PV/T collector is 1.2 times higher than the velocity of the airflow that passes through a wider PV/T collector. It is necessary to make use of the following equation to determine the velocity of the airflow:

$$v_{air} = 1.696 + 0.003903\, I - 0.2162\, T_{amb} - 7.523\times10^{-7}\, I^2 - 6.719\times10^{-5}\, I\, T_{amb} + 0.004525\, T_{amb}^{\,2},\qquad R^2 = 0.9617$$

- The SC integrated with the PV module generates an airflow velocity 252.3% faster than the airflow velocity generated by the SC integrated with the PV module and the EAHE. The airflow velocity is subjected to the following equation:

$$v_{air} = -228.3 + 0.9259\, I + 5.233\, T_{amb} - 0.001332\, I^2 - 0.01941\, I\, T_{amb} + 7.847\times10^{-7}\, I^3 + 2.384\times10^{-5}\, I^2\, T_{amb} - 1.481\times10^{-10}\, I^4 - 9.713\times10^{-9}\, I^3\, T_{amb},\quad R^2 = 0.8699$$

- The airflow velocity caused by the SC through the EAHE with a length of 5 m is 14.7% more than the airflow velocity through the EAHE with a length of 10 m. The following equation establishes the airflow velocity:

$$v_{air} = -2.173 + 0.001843\, I + 0.1288\, T_{amb} - 4.726\times10^{-5}\, I\, T_{amb} - 0.001891\, T_{amb}^{\,2},\qquad R^2 = 0.9731$$

- The airflow velocity that is created by the PV-SC-EAHE system in Al-Najaf is noticeably 20% faster when compared to the airflow velocity that is generated by the PV-SC-EAHE system in Gödöllő. The following equation is put into effect to the airflow velocities in order to perform the estimation:

$$v_{air} = 0.2762 + 0.005205\, I - 0.0423\, T_{amb} - 1.158\times10^{-5}\, I^2 + 0.0001367\, I\, V + 8.533\times10^{-9}\, I^3 - 1.166\times10^{-7}\, I^2\, T_{amb},\qquad R^2 = 0.9627$$

4. *The effect of the forced air and earth-air heat exchanger on the photovoltaic module efficiency.*

I have found that the speed normally generated by the SC alone (without additional SAC) is insufficient to generate sufficient airflow to cool the integrated PV module. For reasons related to the loss of pressure that occurs along the path through which the air passes through the EAHE and the PV/T collector to reach the SC, which dissipates part of the generated velocity on the one hand, and as a result of the insufficient temperature difference between the inside of the SC and the ambient temperature which reduces of the buoyant force inside the SC on the other hand. Therefore, the flow necessary to cool the PV module is not generated. For this reason, one of the proposed methods is to combine the hybrid system (PV-SC-EAHE) with forced airflow using fans, which would cause an increase in the electrical energy generated by the integrated PV modules. However, the forced speed must not be less than 1 m/s or 1.5 m/s, as the increase in generated power is not less than 37.1 W and 35.4 W, respectively. The additional power generated by the integrated PV module was subject to the following equation:

$$P_{pv\text{-}add} = P_{pv} - P_{pv\text{-}ref} = -0.7054 + 1.087 \times v_{fan} - 0.02717\, P_{fan}\,, \quad R^2 = 0.9999$$

In this case, power was generated from the PV module, but at the same time, power was consumed from another source to operate the fans, which is not less than 3 W at a fan speed of 1 m/s and 4.6 W at a fan speed of 1.5 m/s. This necessitates the exploration of an alternative approach to generate sufficient airflow without relying on electrical energy consumption, aiming to enhance the efficiency of PV modules through the utilization of an innovative hybrid system combining PV modules and SC with EAHE (PV-SC-EAHE). The focus of this alternative method should be directed towards elevating the temperature of the air exiting the PV/T collector and entering the SC, ensuring that the average air temperature inside the SC is maximized compared to T_{amb}.

5. *The effect of the solar air collector on the efficiency of photovoltaic modules.*

I have explored that the temperature of the air exiting the PV/T collector and entering the SC is not sufficient to create an adequate flow to draw air from the EAHE, passing through the PV/T, and reaching the SC. This requires raising the temperature of the air before it enters the SC by incorporating a SAC. Therefore, I found that the airflow velocity is directly proportional to the length of the SAC, which means that as the length of the SAC increases, the airflow rate increases and is subject to the equation:

$$v_{air} = 0.0599\, L_{coll} + 0.4564\,, \quad R^2 = 0.9819$$

The airflow rate was 0.47 m/s when the length of the collector was equal to the length of the PV module (the collector's width is similar to the PV module's width). When the length of the SAC became ten times the length of the PV module, the velocity became equal to 1.03 m/s, which is sufficient at this value to

sufficiently cool the PV module and increase the amount of power output compared to the non-integrated PV module. The length of the SAC, which is equal to six times the length of the PV module, was sufficient to generate sufficient air velocity to cool the integrated PV module. This collector, of this size, caused a speed of 0.84 m/s to draw air from the EAHE at a low temperature of 20.8 °C, while the air temperature was not less than 30 °C.

The amount of power output from the PV module increased with the increase in the length of the SAC, as its amount was 37.4 W when the length of the collector was equal to the length of the PV module. Still, when the length of the collector was ten times the length of the PV module, the power increased by 2.2%. This occurred due to increased airflow, which helped reduce the temperature of the PV module from 58.9 °C to 56 °C. The generated power and temperature of the PV module with the SAC and the hybrid system (PV-SC-EAHE) are governed by the following equations, respectively.

$$P_{PV} = 37.335\, L_{coll}^{0.0077} \quad , \quad R^2 = 0.9822$$

$$T_{PV} = 0.0226\, {L_{coll}}^2 - 0.5569\, L_{coll} + 59.326 \, , \quad R^2 = 0.9983$$

6. *The effect of geometric configuration of an earth-air heat exchanger system on its efficiency.*

Based on experimental and simulation results, I have discovered that the efficiency of EAHE is affected by its geometric configuration by comparing four types of geometric configurations of EAHE (S-EAHE, M-EAHE, MS-EAHE, and TS-EAHE systems). Accordingly, the MS-EAHE has the lowest pressure loss among other EAHE system types, resulting in the least additional air fan power required to operate the fan needed to circulate the air inside it. M-EAHE had more significant pressure losses compared to MS-EAHE by approximately 1.6 times. The S-EAHE and TS-EAHE types had the highest pressure losses. They required the most significant amount of additional air fan power for operation, as their pressure losses were 13.8 and 14.7 times, respectively, and their additional air fan power was 71.1 and 75.5 times higher than MS-EAHE. Furthermore, the S-EAHE and TS-EAHE have the highest cooling potential compared to other EAHE system types, at 278.3 W on average. The MS-EAHE and the M-EAHE have less cooling potential of 19.1% and 22.3%, respectively, compared to the S-EAHE and the TS-EAHE types. The four types are subject to the following equations, where CP represents the cooling potential of the EAHE types and T_{in} represents the inlet temperature of the EAHE.

$CP = 1.853\times10^4 \sin(0.002276\, T_{in} + 6.218), \quad R^2=1$ (For S-EAHE and TS-EAHE)

$CP = 1.295\times10^4 \sin(0.002528\, T_{in} + 6.211), \quad R^2=1$ (For M-EAHE)

$CP = 1.383\times10^4 \sin(0.002467\, T_{in} + 6.213), \quad R^2=1$ (For MS-EAHE)

6. SUMMARY

THE EFFECT OF INTEGRATING AN EARTH-AIR HEAT EXCHANGER ON PHOTOVOLTAIC MODULE EFFICIENCY IN COMBINATION WITH A SOLAR CHIMNEY

The study focused on evaluating the efficiency of a combined photovoltaic (PV) module, earth-air heat exchanger (EAHE), and solar chimney (SC) system under extreme climatic conditions in Hungary and Iraq. In Gödöllő, Hungary, two hybrid systems incorporating PV modules, SC, and EAHE, along with a reference system without these components, were meticulously developed and tested. The experimental and simulation results highlighted the superiority of a hybrid system that integrated EAHE, PV/T, SC, and a solar air collector (SAC) when compared to a reference PV module.

The study introduced innovative laboratory and theoretical simulation methods to assess multi-layer soil thermo-physical properties based on moisture content and densities. The developed MATLAB simulation model for PV-SC-EAHE system design and global performance estimation demonstrated a 6.4% difference from measured data, establishing its dependability. Among the four EAHE types, MS-tubed EAHE exhibited the lowest pressure losses and air fan power, while TS-tubed EAHE showed the highest pressure losses, requiring the most power. The multi-tube type had the lowest cooling potential, and EAHE MS-tubes exhibited the highest.

Integration of SC, PV module, and EAHE significantly increased airflow velocity within the tube by 5.3 times. The length of EAHE influenced natural airflow, with EAHE-5 m generating 14.7% faster airflow than EAHE-10 m. Experimental findings revealed that a rectangular SC increased airflow velocity by 5% compared to a circular SC.

Experimental tests indicated that the natural airflow generated by SC, combined with PV-SC-EAHE, was insufficient to cool the PV module, necessitating the integration of SAC before SC and after PV/T. Integration of SAC, with an area ten times that of the PV module, improved PV module efficiency by 2.2%. Simulation results indicated a 20% faster natural airflow in the hot location (Al-Najaf) compared to the colder location (Gödöllő), with maximum velocities of 1.1 m/s and 0.95 m/s, respectively.

Temperature differentials between air and soil at a depth of 2 m during summer and winter were measured, with Gödöllő experiencing higher differentials than Al-Najaf. In Al-Najaf, soil temperature at a depth of 5 m remained consistent throughout the year, with significant temperature differences between soil and air.

7. IMPORTANT PUBLICATIONS RELATED TO THE THESIS

Refereed papers in foreign languages:

1. **Ali, M. H.**, Kurjak, Z., & Beke, J. (2020): Evaluation of the temperature effect on the outputs and efficiency of photovoltaic (PV) cell by using Simulink/MATLAB, Mechanical Engineering Letters, Gödöllő, Hungary, Vol. 20, pp. 59-66, HU ISSN 2060-3789
2. **Ali, M. H.,** Kurjak, Z., & Beke, J. (2021): Experimental evaluation of the underground soil temperature readiness for heating and cooling systems installation, European Journal of Energy Research, Vol. 1, pp. 1-6, ISSN 2506-8016. https://doi.org/10.24018/ejenergy.2021.1.2.8
3. **Ali, M. H.**, Kurjak, Z., & Beke, J. (2022): Simulation Modeling for Earth to Air Heat Exchanger System by Using MATLAB, European Journal of Engineering Science and Technology, Vol. 5, pp. 1-19, ISSN 2538-9181. https://doi.org/10.33422/ejest.v5i1.843
4. **Ali, M. H.**, Kurjak, Z., & Beke, J. (2023): Investigation of earth air heat exchangers functioning in arid locations using Matlab/Simulink, Renewable Energy, Vol. 209, pp. 632-643, ISSN 2506-8016. https://doi.org/10.1016/j.renene.2023.04.042 (Scopus: Q1/D1, IF: 8.7)
5. **Ali, M. H.**, Kurjak, Z., & Beke, J. (2023): Modelling and simulation of solar chimney power plants in hot and arid regions using experimental weather conditions, International Journal of Thermofluids, Vol. 20, pp.100434, ISSN 2666-2027. (Scopus: Q1/D1)
   https://doi.org/10.1016/j.ijft.2023.100434

International conference proceedings:

6. **Ali, M. H.**, Kurjak, Z., & Beke, J. (2020): Experimental evaluation of the groundwater temperature readiness for heating and cooling systems installation in subtropical region, 12th International Symposium on Exploitation of Renewable Energy Sources and Efficiency, Subotica, Serbia, April 16-18, 2020, P. 18, ISBN: 978-86-919769-7-2.

International conference abstracts:

7. **Ali, M. H.**, Kurjak, Z., & Beke, J. (2020): Enhancement the efficiency of photovoltaic solar cell by using combination earth-air heat exchanger with assist solar chimney, Book of Abstracts, 26th Workshop on Energy and Environment, Gödöllő, Hungary, December 10-11, 2020, p. 18., ISBN 978-963-269-928-8.
8. **Ali, M. H.,** Kurjak, Z., & Beke, J. (2021): Impact a Combination of Solar Energy and Geothermal Systems on PV Output Power, Book of Abstracts, 20th International Workshop for Young Scientists, BioPhys Spring 2021, Prague, Czech Republic, May 18, 2021, p. 56, ISBN 978-83-89969-68-2.
9. **Ali, M. H.**, Kurjak, Z., & Beke, J. (2023): The effect of forced airflow inside the solar chimney on the photovoltaic module power generation, Book of Abstracts, 29th Workshop on Energy and Environment, Gödöllő, Hungary, December 7-8, 2023, p. 13., ISBN 978-963-623-079-1.